Journal of Solid State Chemistry 182 (2009) 2815–2821

Contents lists available at ScienceDirect

Journal of Solid State Chemistry

journal homepage: www.elsevier.com/locate/jssc

Oxygen vacancy ordering within anion-deficient Ceria

S. Hull [a,*], S.T. Norberg [a,b], I. Ahmed [a,b], S.G. Eriksson [b], D. Marrocchelli [c], P.A. Madden [c,d]

[a] The ISIS Facility, Rutherford Appleton Laboratory, Chilton, Didcot, Oxfordshire OX11 0QX, UK
[b] Department of Chemical and Biological Engineering, Chalmers University of Technology, SE-412 96 Gothenburg, Sweden
[c] School of Chemistry, Edinburgh University, The King's Building, West Mains Road, Edinburgh EH9 3JJ, UK
[d] Department of Materials, University of Oxford, Parks Road, Oxford OX1 3PH, UK

ARTICLE INFO

Article history:
Received 18 June 2009
Received in revised form
22 July 2009
Accepted 24 July 2009
Available online 3 August 2009

Keywords:
Crystal defects
Neutron diffraction
Diffuse scattering
Ionic conduction
Oxygen vacancies

ABSTRACT

The structural properties of anion deficient ceria, $CeO_{2-\delta}$, have been studied as a function of oxygen partial pressure, $p(O_2)$, over the range $0 \geq \log_{10} p(O_2) \geq -18.9$ at 1273(2) K using the neutron powder diffraction technique. Rietveld refinement of the diffraction data collected on decreasing $p(O_2)$ showed increases in the cubic lattice parameter, a, the oxygen nonstoichiometry, δ, and the isotropic thermal vibration parameters, u_{Ce} and u_O, starting at $\log_{10} p(O_2) \sim -11$. The increases are continuous, but show a distinct kink at $\log_{10} p(O_2) \sim -14.5$. Analysis of the total scattering (Bragg plus diffuse components) using reverse Monte Carlo (RMC) modelling indicates that the O^{2-} vacancies preferentially align as pairs in the $\langle 111 \rangle$ cubic directions as the degree of nonstoichiometry increases. This behaviour is discussed with reference to the chemical crystallography of the CeO_2–Ce_2O_3 system at ambient temperature and, in particular, to the nature of the long-range ordering of O^{2-} vacancies within the crystal structure of Ce_7O_{12}.

1. Introduction

Solid oxide fuel cells (SOFCs) are a key technology in the strategy to develop more environmentally benign power sources. A critical component within an SOFC device is the solid electrolyte, which transfers O^{2-} ions from the air side (cathode) to the fuel side (anode) of the device, with charge balance maintained by the motion of electrons in the reverse direction through an external circuit, which is exploited as electrical power. Two major requirements of the solid electrolyte are, therefore, a high oxide-ion conductivity, σ_i, and a low electronic conductivity, σ_e, with the latter essential to avoid internal short-circuits. Currently, the material most widely used for the role of solid electrolyte in SOFCs is yttria stabilised zirconia (YSZ, of formula $Zr_{1-x}Y_xO_{2-x/2}$ with $x \sim 0.15$) [1]. However, SOFCs must generally be operated at temperatures of ~1200 K to achieve the required level of ionic conductivity within the YSZ electrolyte and the potential advantages of operation at lower temperatures of around 600–900 K, which include reduced problems of corrosion, sealing and start-up times, have motivated considerable research effort to identify materials with higher values of σ_i than YSZ. These include ZrO_2 doped with other trivalent species (such as Sc^{3+} [2]), isovalently doped Bi_2O_3 (including $Bi_{1-x}Y_xO_{3/2}$ with $x \sim 0.25$ [3]) and aliovalently doped CeO_2 (such as $Ce_{1-x}Sm_xO_{2-x/2}$ with $x \sim 0.2$ [4]). All these compounds, including YSZ, possess the cubic fluorite crystal structure (space group $Fm\bar{3}m$), which can be described as cations occupying alternate cube centres within a simple cubic array of anions (see Fig. 1) or as anions occupying all the tetrahedral interstices within a face centred cubic (*f.c.c.*) array of cations. Significantly, these compounds are also anion deficient, with a high concentration of oxygen vacancies which play a central role in promoting the macroscopically observed ionic conductivity.

Many of the candidate materials mentioned above have a potential drawback, owing to the onset of electronic conduction under the strongly reducing atmospheres experienced on the fuel side of the SOFC. This is particularly true of the CeO_2 based systems [4–7]. Nonstoichiometric $CeO_{2-\delta}$ is predominantly an electronic n-type semiconductor at elevated temperatures [8–10], with the ionic contribution to the total conductivity reported to be only a few percent [11]. The replacement of some of the Ce^{4+} with Ce^{3+} is compensated by the inclusion of anion vacancies [12], with X-ray diffraction studies showing that the alternative mechanism involving cation interstitials accounts for $<0.1\%$ of the total defect concentration [13]. Ionic conduction is then a consequence of anion motion via a vacancy diffusion mechanism between nearest neighbour sites in $\langle 100 \rangle$ directions [14].

The phase diagram of the $CeO_{2-\delta}$ system has been extensively studied and a number of crystalline phases are formed at temperatures less than around 700 K in which the anion vacancies are long-range ordered within the lattice (see, for example, [15–24]). Compounds of stoichiometry $Ce_{32}O_{58}$, $Ce_{32}O_{56}$ and

* Corresponding author. Fax: +44 1235 445720.
E-mail address: stephen.hull@stfc.ac.uk (S. Hull).

0022-4596/$ - see front matter © 2009 Elsevier Inc. All rights reserved.
doi:10.1016/j.jssc.2009.07.044

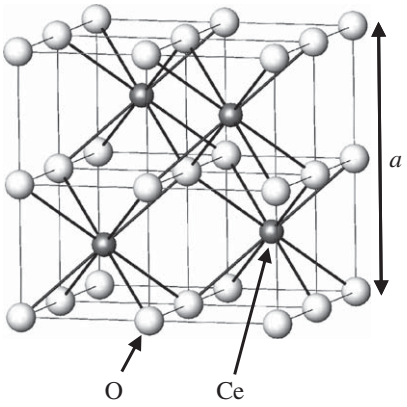

Fig. 1. The cubic fluorite structure of stoichiometric CeO_2. The space group is $Fm\bar{3}m$, with cations at the 4(a) sites at 0,0,0, *etc.* and the oxygen atoms at the 8(c) sites at 1/4, 1/4, 1/4, etc.

$Ce_{32}O_{55}$ were originally reported, but their compositions were subsequently corrected to $Ce_{11}O_{20}$, Ce_9O_{16} and Ce_7O_{12}, respectively (see [21,22] and references therein). The observation of superlattice lines in neutron diffraction patterns supported the presence of these phases, plus another of stoichiometry $Ce_{10}O_{18}$, with the four compounds suggested to be the $n = 7$, 9, 10 and 11 members of a homologous series of composition Ce_nO_{2n-2} [20]. The $n = 7$ and 11 compounds have also been observed in specific heat and electron microscopy studies, with evidence for additional phases with compositions close to $Ce_{19}O_{34}$ and $Ce_{62}O_{112}$ [17,18]. The crystal structures of the $n = 4$, 7 and 11 members (Ce_2O_3, Ce_7O_{12} and $Ce_{11}O_{20}$, respectively) have been determined and the nature of the O^{2-} vacancy ordering schemes discussed [19,25]. At higher temperatures, long-range ordering of the vacancies is lost and an anion-deficient cubic fluorite structured phase is stable down to a nonstoichiometry of $\delta \sim 0.29$ at 1273 K [23]. A number of studies of the lattice expansion of $CeO_{2-\delta}$ as a function of oxygen partial pressure, $p(O_2)$, have been published using X-ray diffraction and dilatometry techniques [12,26–29]. At temperatures in the region of 1273 K, significant expansion of the lattice is observed at $\log_{10} p(O_2)$ values $\lesssim -11$, though there are some differences between the various results reported. The most recent study showed a marked change in the lattice expansivity at $\delta \sim 0.06$ and 1273 K, which was suggested to arise from short-range ordering of the anion vacancies within the cubic fluorite lattice as their concentration increases [29].

This paper describes a neutron powder diffraction study of the structural behaviour of $CeO_{2-\delta}$ as a function of nonstoichiometry, with Rietveld refinement of the Bragg scattering used to investigate the time-averaged crystal structure and reverse Monte Carlo (RMC) analysis of the total scattering (Bragg plus diffuse scattering) used to probe the short-range correlations between the O^{2-} vacancies.

2. Experimental details

Powdered, stoichiometric CeO_2 of stated purity 99.995% was supplied by the Aldrich Chemical Company and formed into 20 pellets, each of 6 mm diameter and 2–3 mm thickness. These discs were stacked vertically on top of a porous silica glass frit within a silica glass tube of wall thickness 0.5 mm. This tube passes vertically through the hot zone of a resistive heating furnace designed for neutron powder diffraction experiments, constructed using vanadium foil heating element and heat shields. All measurements were performed at a temperature of 1273(2) K, with gas flowing through the silica tube at a rate of 80 sccm. Gas mixtures of O_2, Ar, CO_2 and CO were used to provide variable oxidising/reducing atmosphere around the sample pellets, with the gas flow and composition controlled by a gas panel (Hastings 300 series mass flow controllers) interfaced to the control PC of the diffractometer. The temperature and partial pressure of oxygen within the silica tube was monitored using a type DS zirconia sensor supplied by Australian Oxytrol Systems. Measurements were started under an atmosphere of pure O_2 gas ($\log_{10} p(O_2) \sim 0$), with the sample gradually reduced to $\log_{10} p(O_2)$ of -18.9 (obtained with pure CO gas). A more detailed description of the sample cell, gas panel and control system can be found elsewhere [30].

The diffraction experiments were performed using the Polaris powder diffractometer at the ISIS Facility, Rutherford Appleton Laboratory, UK [31]. Diffraction data were collected using the backscattering detector bank which covers the scattering angles $130^\circ < 2\theta < 160^\circ$ (providing data over the d-spacing range $0.2 < d(\text{Å}) < 3.2$ with a resolution $\Delta d/d \sim 5 \times 10^{-3}$) and the low-angle detector bank situated at $28^\circ < 2\theta < 42^\circ$ (providing data over the d-spacing range $0.5 < d(\text{Å}) < 8.3$ with a resolution of $\Delta d/d \sim 10^{-2}$). Two data collection runs were performed as a function of oxygen partial pressure. In the first, diffraction data were collected for approximately 15 min at 45 different $p(O_2)$ values, with data collection started 5 min after changing the gas composition to allow equilibration. This provided data of sufficient statistical quality to allow Rietveld profile refinement of the data to be performed using the GSAS software [32], to extract the variation of the cubic lattice parameter, a, the oxygen nonstoichiometry, δ in $CeO_{2-\delta}$, and the isotropic thermal vibration parameters of the two species, u_{Ce} and u_O. Additional fitted parameters for each detector bank comprised a scale factor, peak width parameters describing Gaussian and Lorentzian contributions to the Bragg profile and the coefficients of a 15th order shifted Chebyshev polynomial function to describe the background scattering, which predominantly arises from the silica glass tube.

The measured scattering between the Bragg peaks also contains weak diffuse scattering, which contains information concerning short-range ion–ion correlations within the sample. This aspect was studied in a second run (starting with newly prepared pellets) with significantly longer data collections (10–12 h) performed at $\log_{10} p(O_2)$ values of $-8.4(2)$, $-14.1(2)$, $-15.5(2)$ and $-18.9(2)$. The data were corrected for the effects of beam attenuation and background scattering from the silica tube and furnace using the program Gudrun [33], to give the total scattering function, $S(Q)$ (where the scattering vector Q is related to the interplanar spacing (d-spacing) by $Q = 2\pi/d$). Fourier transform of $S(Q)$ gives the total radial distribution function, $G(r)$, which is the sum of the individual radial distribution functions, $g_{ij}(r)$, for each pair of ionic species, weighted by a factor $c_i c_j b_i b_j$ (where c_i and b_i are the concentration and neutron scattering length of species i, respectively). Reverse Monte Carlo (RMC) simulations were performed using the RMCProfile software [34] with configuration boxes of $10 \times 10 \times 10$ unit cells. The positions of the ions are then adjusted randomly, one at a time and subject to periodic boundary conditions, to obtain the best fit to both the real space data (fitting to $G(r)$) and the reciprocal space data (fitting to $S(Q)$), whilst also using the Bragg profile to provide the constraint of long-range crystallinity. Since the $S(Q)$ is calculated within the RMCProfile code by Fourier transformation of the $G(r)$ determined from the (finite) simulation box, it will be broadened in Q due to the limited range of r. As a result, it is necessary to convolve the experimental $S(Q)$ with a box function to obtain $S_{box}(Q)$ using the expression

$$S_{box}(Q) = \frac{1}{\pi} \int_{-\infty}^{\infty} S(Q') \frac{\sin L(Q - Q')/2}{Q - Q'} dQ',$$

where L is the size of the simulation box.